Beampattern Analysis for MIMO Radar and Telecommunication System Coexistence

Awais Khawar, Ahmed Abdel-Hadi, T. Charles Clancy, and Robert McGwier

Bradley Dept of Electrical and Computer Engineering
Virginia Tech, Arlington, VA, 22203, USA

Email:{awais, aabdelhadi, tcc, rwmcgwi}@vt.edu

***Abstract*—In this paper, we present a beampattern analysis of the MIMO radar coexistence algorithm proposed in [1]. We extend the previous work and analyze the performance of MIMO radars by projecting finite alphabet constant-envelope waveforms onto the null-space of interference channel matrix. First, we compare and analyze the Crameŕ-Rao bound (CRB) on angle direction estimation. Second, we compare and analyze beampatterns of the original radar waveform and the null-projected radar waveform. Analytical and simulation results show minimal degradation of a radar's angle estimation of a target and transmit-receive beampattern. We also propose methods to substantially improve angle estimation and beampatterns of a null projected radar waveform which will not only guarantee optimal performance of the radar but at the same time guarantee coexistence of the radar and communication systems.**

***Index Terms*—spectrum sharing, coexistence, MIMO radar, beampattern**

I. Introduction

The United States government is exploring ways to share spectrum, currently in-use by the federal agencies, for commercial utilization in order to satisfy the huge bandwidth demands by consumers and business broadband users. In recent studies conducted by the National Telecommunications and Information Administration (NTIA), along with the FCC, it has been noticed that huge chunks of spectrum reserved for the federal agencies goes unused. This initiative will result in huge economic and social prospects for the nation. However, innovative approaches need to be seeked in order to enable sharing of the federal spectrum without compromising sensitive or classified information or operations.

One of the many spectrum bands identified by the FCC for a possible sharing is the 3500-3650 MHz band where the Department of Defense (DoD) operates many radars. A launch of commercial communication systems would result in unwanted electromagnetic interference (EMI) which can jeopardize the radar mission. Therefore, novel techniques are needed to enable spectrum sharing between a radar and a communication system. One such technique was proposed by Shabnam et al. [1] to share a radar's spectrum with a commercial communication system, e.g., WiMAX or LTE, in the spatial domain. The authors proposed projecting MIMO radar waveform onto the null-space of interference channel matrix between the MIMO radar and MIMO communication system. Lackpour et. al. [2] proposed spatial, spectral, temporal, and system level interference mitigation techniques between WiMax systems and ground based radars. Deng et al. proposed a signal processing approach for interference mitigation from wireless communication systems to MIMO radar by using a beamforming approach for MIMO radar [3]. NTIA also lists many solutions to mitigate interference from communication systems to radars operating in the 2700-2900 MHz band [4]. Other related work can be found in [1] and references therein.

The remainder of this paper is organized as follows. Section II discusses system architecture. In Section III, we design finite alphabet constant-envelope (FACE) radar waveforms. In Section IV, we explain the null-space projection algorithm. Section V derives the analytical expressions for CRB and transmit-receive beampatterns for null-projected radar waveform. Section VI discusses simulation setup and provides quantitative results along with the discussion. Section VII concludes the paper.

II. System Architecture

In this paper, we consider a colocated MIMO radar, with M_T transmit antennas and M_R receive antennas, and a MIMO communication system, with N_R receive antennas. The colocated radars have an antenna spacing on the order of half the wavelength of the carrier which gives better target parameter identifiability, improved spatial resolution, but poor spatial diversity as compared to widely-spaced radars [5]. The radar and communication systems are the co-primary users of the 3.6 GHz band under consideration. A typical coexistence scenario is shown in Fig. 1 where the MIMO radar is illuminating a target while projecting its signal onto the null space of interference channel $\mathbf{H}_{N_R\times M_T}$ between the radar and the communication system and $\mathbf{H}_{M_R\times M_T}$ is the target impulse response matrix. If $\mathbf{x}(t)$ is the signal transmitted from a radar, then the received signal at a communication system receiver can be written as

$$\mathbf{y}(t) = \mathbf{H}_{N_R\times M_T}\mathbf{x}(t) + \mathbf{w}(t) \tag{1}$$

where $\mathbf{w}(t)$ is the additive white Gaussian noise and the goal of a radar is to map its signals onto the null-space of $\mathbf{H}_{N_R\times M_T}$ in order to avoid interference to a communication system.

978-1-4799-2358-8/14/$31.00 ©2014 IEEE

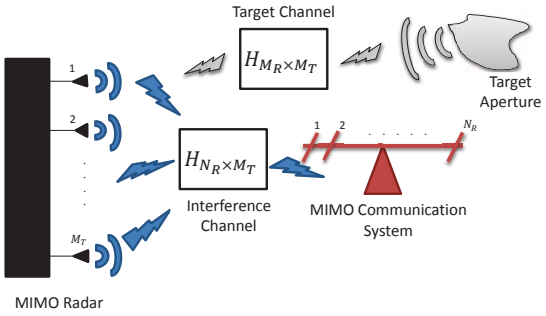

Fig. 1. Block diagram of the MIMO communication system and interfering MIMO radar

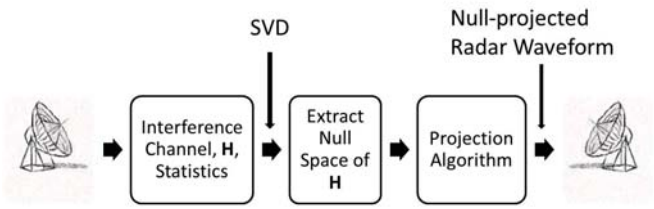

Fig. 2. System Architecture

III. FACE MIMO Radar Waveforms

The capability of a MIMO radar to have a diverse set of waveforms and its ability to optimize waveforms according to a desired transmit-receive beampatterns make it superior to a phased array radar [6]. In this paper, we consider FACE radar waveforms designed according to the following constraints

$$C_1 : \mathbf{y}^H \mathbf{R}_x \mathbf{y} \geq 0, \forall \mathbf{y}$$
$$C_2 : \mathbf{R}_x(m,m) = 1 \qquad m = 1, 2, \ldots, M_T$$

where C_1 guarantees that the covariance matrix is a positive-semidefinite matrix and C_2 guarantees that all the antennas transmit unit power waveforms. The constant-envelope property of the waveform is important in order to allow radio frequency amplifiers to operate at a maximum power efficiency. We synthesize the covariance matrix $\mathbf{R}_x$ by the method of Ahmed et al [7]. Their approach is novel since they transform the problem of finding MIMO radar waveforms to realize a given covariance matrix into finding a Gaussian random variables to realize another covariance matrix using memoryless nonlinear functions [7]. Once $\mathbf{R}_x$ is synthesized, the waveform matrix $\mathbf{X}$, with N samples, can be determined as

$$\mathbf{X} = \mathcal{X} \mathbf{\Lambda}^{1/2} \mathbf{W}^H \tag{2}$$

where $\mathbf{X} = \begin{bmatrix} \mathbf{x}_1 & \mathbf{x}_2 & \ldots & \mathbf{x}_{M_T} \end{bmatrix} \in C^{N \times M_T}$ with $\mathbf{x}_i$ the waveform transmitted from the i^{th} antenna, $\mathcal{X} \in C^{N \times M_T}$ is a matrix of zero mean and unit variance Gaussian random variables, $\mathbf{\Lambda} \in \mathcal{R}^{M_T \times M_T}$ is the diagonal matrix of eigenvalues and $\mathbf{W} \in C^{M_T \times M_T}$ is the matrix of eigenvectors of $\mathbf{R}_x$ [7]. The distribution in the columns of $\mathbf{X}$ is Gaussian. We are interested in BPSK waveforms because of their low sidelobes. In order to generate BPSK random variables to realize $\mathbf{R}_x$, the Gaussian random variables x_m can be mapped onto BPSK symbol z_m

$$z_m = sign(x_m), \quad m \in \{1, 2, \ldots, M_T\}. \tag{3}$$

Once we design the BPSK waveforms we can write the signal covariance matrix as

$$\mathbf{R}_x = \int_{T_0} \mathbf{x}(t)\mathbf{x}^H(t)dt = \begin{bmatrix} 1 & \gamma_{12} & \cdots & \gamma_{1M_T} \\ \gamma_{21} & 1 & \cdots & \gamma_{2M_T} \\ \vdots & \vdots & \ddots & \vdots \\ \gamma_{M_T 1} & \gamma_{M_T 2} & \cdots & 1 \end{bmatrix} \tag{4}$$

where $\mathbf{x}(t) = \begin{bmatrix} x_1(t) & x_2(t) & \cdots & x_{M_T}(t) \end{bmatrix}$, $0 \leq |\gamma_{ij}| \leq 1$ is the complex correlation coefficient between the i^{th} and j^{th} transmitted signal, and the phases of γ_{ij}, $\{i, j\} \in \{1, 2, \ldots, M_T\}$, control the transmitted beam direction, and T_0 is the observation interval.

First, we are interested in finite-alphabet constant-envelope orthonormal waveforms. For orthonormal waveforms, $\gamma = 0$. Orthonormal waveforms results in omnidirectional signal transmission thus illuminating all angles. Thus, the signal correlation matrix is an identity matrix, $\mathbf{R}_x = \mathbf{I}_{M_T}$.

Second, we are interested in finite alphabet constant-envelope coherent waveforms. The coherent waveforms, $\gamma = 1$, obey

$$\mathbf{x}(t) = \mathbf{a}_T^*(\theta_0)x(t) \tag{5}$$

where $x(t)$ is the scalar transmit waveform. The beam is steered to desired direction θ_0 by the phases of $\mathbf{a}_T^*(\theta_0)$. By substituting (5) in (4) we get

$$\mathbf{R}_x = \int_{T_0} \left(\mathbf{a}_T^*(\theta_0)x(t)\right)\left(\mathbf{a}_T^*(\theta_0)x(t)\right)^H dt = \mathbf{a}_T^*(\theta_0)\mathbf{a}_T^T(\theta_0). \tag{6}$$

IV. Spatial Coexistence through Null-Space Transmission

Null space based coexistence mechanisms, for cognitive radios, have been proposed previously by many researchers [8], [9]. To exploit transmission over null-space of the interference channel $\mathbf{H}$, the first step for the MIMO radar is to estimate the interference channel, as shown in Figure 2. In this paper, we assume that the communication system can periodically inform the radar systems of its status, through a cognitive pilot channel (CPC) [10]. After the channel matrix $\mathbf{H}$ is estimated, the next step is to find the null space of $\mathbf{H}$. The null space of any matrix can be computed by using singular value decomposition (SVD) theorem. For the complex channel matrix $\mathbf{H}$ the SVD is given as

$$\mathbf{H}_{N_R \times M_T} = \mathbf{U}_{N_R \times N_R} \mathbf{\Sigma}_{N_R \times M_T} \mathbf{V}^H_{M_T \times M_T} \tag{7}$$

where $\mathbf{U}$ is the complex unitary matrix, $\mathbf{\Sigma}$ is the diagonal matrix of singular values, and $\mathbf{V}^H$ is the complex unitary matrix.

The columns of $\mathbf{V}$ corresponding to vanishing singular values in matrix $\mathbf{\Sigma}$ span the null space of $\mathbf{H}$. We denote this by $\check{\mathbf{V}}$. Next, we present an analysis of effects if the radar transmits on the null space of $\mathbf{H}$ to avoid interference with

the communication system [1]. The radar signal projected onto null space of $\mathbf{H}$ can be written as

$$\check{\mathbf{x}} = \mathbf{P}_{\check{\mathbf{V}}}\mathbf{x} \tag{8}$$

where

$$\mathbf{P}_{\check{\mathbf{V}}} = \check{\mathbf{V}}(\check{\mathbf{V}}^H\check{\mathbf{V}})^{-1}\check{\mathbf{V}}^H \tag{9}$$

is the projection matrix onto the null space of $\mathbf{H}$, which is spanned by columns of $\check{\mathbf{V}}$. It is easy to verify that the projection matrix defined here satisfies the properties, $\mathbf{P}_{\check{\mathbf{V}}} = \mathbf{P}^T_{\check{\mathbf{V}}}$ and $\mathbf{P}_{\check{\mathbf{V}}} = \mathbf{P}^2_{\check{\mathbf{V}}}$, of a projection matrix [11].

V. Analysis

A. Crameŕ-Rao bound (CRB): The Crameŕ-Rao bound is the lower bound on the mean square error (MSE) of unbiased estimators. The CRB for single target's, no interference case, direction estimation is given, as [6], by

$$\mathrm{CRB}(\theta) = \frac{1}{2\mathrm{SNR}}\Bigg(M_R\dot{\mathbf{a}}_T^H(\theta)\mathbf{R}_x^T\dot{\mathbf{a}}_T(\theta) + \mathbf{a}_T^H(\theta)\mathbf{R}_x^T\mathbf{a}_T(\theta)\|\dot{\mathbf{a}}_R(\theta)\|^2 - \frac{M_R\left|\mathbf{a}_T^H(\theta)\mathbf{R}_x^T\dot{\mathbf{a}}_T(\theta)\right|^2}{\mathbf{a}_T^H(\theta)\mathbf{R}_x^T\mathbf{a}_T(\theta)}\Bigg)^{-1}. \tag{10}$$

B. Beampatterns: In this section we derive analytical results of transmit-receive beampatterns for FACE MIMO radar waveform projected onto the null-space of the interference channel matrix $\mathbf{H}$. The transmit and receive beampatterns, which measure the beamformer's response to a target at direction θ, when the beam is steered digitally to a direction θ_D, for MIMO radar in terms of transmit and receive steering vectors are given, as [6], by

$$G_{\mathrm{Tx}}(\theta,\theta_D) = K_{\mathrm{Tx}}\frac{|\mathbf{a}_T^H(\theta)\mathbf{R}_x^T\mathbf{a}_T(\theta_D)|^2}{\mathbf{a}_T^H(\theta_D)\mathbf{R}_x^T\mathbf{a}_T(\theta_D)} \tag{11}$$

and

$$G_{\mathrm{Rx}}(\theta,\theta_D) = K_{\mathrm{Rx}}\frac{|\mathbf{a}_R^H(\theta)\mathbf{a}_R(\theta_D)|^2}{M_R} \tag{12}$$

where K_{Tx} and K_{Rx} are normalization constants. The composite transmit-receive pattern can be jointly written as

$$G_{\mathrm{Tx,Rx}}(\theta,\theta_D) = K_{\mathrm{Tx,Rx}}\frac{|\mathbf{a}_T^H(\theta)\mathbf{R}_x^T\mathbf{a}_T(\theta_D)|^2}{\mathbf{a}_T^H(\theta_D)\mathbf{R}_x^T\mathbf{a}_T(\theta_D)}\frac{|\mathbf{a}_R^H(\theta)\mathbf{a}_R(\theta_D)|^2}{M_R} \tag{13}$$

where $K_{\mathrm{Tx,Rx}}$ is the normalization constant.

1) Orthonormal Signals: For orthonormal signals $\mathbf{R}_x = \mathbf{I}_{M_T}$, see equation (4), as $\gamma = 0$, substituting in (11) and (13) and using the fact that $\mathbf{a}_T^H(\theta_D)\mathbf{a}_T(\theta_D) = M_T$ we have

$$G_{\mathrm{Tx_{Orth}}}(\theta,\theta_D) = K_{\mathrm{Tx_{Orth}}}\frac{|\mathbf{a}_T^H(\theta)\mathbf{a}_T(\theta_D)|^2}{M_T} \tag{14}$$

and

$$G_{\mathrm{Tx,Rx_{Orth}}}(\theta,\theta_D) = K_{\mathrm{Tx,Rx_{Orth}}}\frac{|\mathbf{a}_T^H(\theta)\mathbf{a}_T(\theta_D)|^2}{M_T}\frac{|\mathbf{a}_R^H(\theta)\mathbf{a}_R(\theta_D)|^2}{M_R}. \tag{15}$$

M_T and M_R can be manipulated to achieve beampatterns having narrower mainlobes and sidelobes and improved angular resolutions.

2) Coherent Signals: For coherent signals $\mathbf{R}_x = \mathbf{a}_T^*(\theta_0)\mathbf{a}_T^T(\theta_0)$, see equation (6), substituting in (11) and (13) we have

$$G_{\mathrm{Tx_{Coh}}}(\theta,\theta_D) = |\mathbf{a}_T^H(\theta)\mathbf{a}_T(\theta_0)|^2 \tag{16}$$

and

$$G_{\mathrm{Tx,Rx_{Coh}}}(\theta,\theta_D) = K_{\mathrm{Coh}}\frac{|\mathbf{a}_T^H(\theta)\mathbf{a}_T(\theta_0)|^2|\mathbf{a}_R^H(\theta)\mathbf{a}_R(\theta_D)|^2}{M_R}. \tag{17}$$

For this case, M_R, only, can be manipulated to achieve beampatterns having narrower mainlobes and sidelobes and improved angular resolutions.

3) Null-space Projected Signals: The radar waveform projected onto the null-space of $\mathbf{H}$ is given by $\check{\mathbf{x}}$, see equation (8), so we can write the correlation matrix of null-projected transmitted signals as

$$\mathbf{R}_{\check{x}} = \int_{T_o}\check{\mathbf{x}}(t)\,\check{\mathbf{x}}^H(t)\,\mathrm{dt} = \begin{bmatrix} 1 & \check{\gamma}_{12} & \cdots & \check{\gamma}_{1M_T} \\ \check{\gamma}_{21} & 1 & \cdots & \check{\gamma}_{2M_T} \\ \vdots & \vdots & \ddots & \vdots \\ \check{\gamma}_{M_T1} & \check{\gamma}_{M_T2} & \cdots & 1 \end{bmatrix} \tag{18}$$

where $\check{\gamma}_{ij}$ is the complex correlation coefficient between the i^{th} and j^{th} transmitted signal, and the phases of $\check{\gamma}_{ij}$, $\{i,j\} \in \{1,2,\ldots,M_T\}$, control the transmitted beam direction. Thus the new transmit beampattern is given by

$$G_{\mathrm{Tx_{Null}}}(\theta,\theta_D) = K_{\mathrm{Tx_{Null}}}\frac{|\mathbf{a}_T^H(\theta)\mathbf{R}_{\check{x}}^T\mathbf{a}_T(\theta_D)|^2}{\mathbf{a}_T^H(\theta_D)\mathbf{R}_{\check{x}}^T\mathbf{a}_T(\theta_D)} \tag{19}$$

and the transmit-receive beampattern is given by

$$G_{\mathrm{Tx,Rx_{Null}}}(\theta,\theta_D) = K_{\mathrm{Tx,Rx_{Null}}}\frac{|\mathbf{a}_T^H(\theta)\mathbf{R}_{\check{x}}^T\mathbf{a}_T(\theta_D)|^2}{\mathbf{a}_T^H(\theta_D)\mathbf{R}_{\check{x}}^T\mathbf{a}_T(\theta_D)}\frac{|\mathbf{a}_R^H(\theta)\mathbf{a}_R(\theta_D)|^2}{M_R}. \tag{20}$$

Comparing equations (15) and (20), we note that the first term in (20) introduces ambiguity in the transmit array gain due to null-projected waveform. For a fixed value of θ and θ_D the ambiguity in the transmit array gain is dependent on the number of transmit antennas, M_T. Increasing the number of receive antennas, M_R, can resolve the ambiguity in the overall composite transmit-receive beampattern by achieving narrower beams. This is also shown through simulation in the next section and summarized in Table I. For analysis, we normalize all beampatterns to one at the maximum point.

Lemma V.1. *For orthonormal signals* $\mathbf{x}(t)$*, such that* $\mathbf{R}_x = \int_{T_0}\mathbf{x}(t)\mathbf{x}^H(t)dt = \mathbf{I}$*,* $G_{Tx}(\theta,\theta_D) \le G_{Tx_{Null}}(\theta,\theta_D)$*.*

Proof: The covariance matrix for projected waveforms is given by equation (18). Consider writing $\mathbf{R}_{\check{x}} = \mathbf{I} + \mathbf{\Gamma}$, where

$$\mathbf{\Gamma} \triangleq \begin{bmatrix} 0 & \check{\gamma}_{12} & \cdots & \check{\gamma}_{1M_T} \\ \check{\gamma}_{21} & 0 & \cdots & \check{\gamma}_{2M_T} \\ \vdots & \vdots & \ddots & \vdots \\ \check{\gamma}_{M_T1} & \check{\gamma}_{M_T2} & \cdots & 0 \end{bmatrix}. \tag{21}$$

We select $K_{\mathrm{Tx_{Orth}}}$ and $K_{\mathrm{Tx_{Null}}}$ such that the denominators of equations (14) and (19) are normalized to unity. Then, using

equation (21), we can write

$$\begin{aligned} G_{\mathrm{Tx_{Null}}}(\theta,\theta_D) &= |\mathbf{a}_T^H(\theta)\mathbf{R}_{\tilde{x}}^T\mathbf{a}_T(\theta_D)|^2 \\ &= |\mathbf{a}_T^H(\theta)(\mathbf{I}+\mathbf{\Gamma})^T\mathbf{a}_T(\theta_D)|^2 \\ &= |\mathbf{a}_T^H(\theta)\mathbf{a}_T(\theta_D)+\mathbf{a}_T^H(\theta)\mathbf{\Gamma}^T\mathbf{a}_T(\theta_D)|^2 \\ &\geq |\mathbf{a}_T^H(\theta)\mathbf{a}_T(\theta_D)|^2 \triangleq G_{\mathrm{Tx_{Orth}}}(\theta,\theta_D) \end{aligned} \quad (22)$$

where equation (22) follows from triangle inequality for complex numbers. ■

Lemma V.2. *For orthonormal signals* $\mathbf{x}(t)$*, such that* $\mathbf{R}_x = \int_{T_0}\mathbf{x}(t)\mathbf{x}^H(t)dt = \mathbf{I}$*,* $G_{Tx,Rx_{Orth}}(\theta,\theta_D) \leq G_{Tx,Rx_{Null}}(\theta,\theta_D)$.

Proof: We select $K_{\mathrm{Tx,Rx_{Orth}}}$ and $K_{\mathrm{Tx,Rx_{Null}}}$ such that the denominators of equations (15) and (20) are normalized to unity. Then, using equation (21), we can write

$$\begin{aligned} G_{\mathrm{Tx,Rx_{Null}}}(\theta,\theta_D) &= |\mathbf{a}_T^H(\theta)\mathbf{R}_{\tilde{x}}^T\mathbf{a}_T(\theta_D)|^2|\mathbf{a}_R^H(\theta)\mathbf{a}_R(\theta_D)|^2 \\ &= |\mathbf{a}_T^H(\theta)(\mathbf{I}+\mathbf{\Gamma})^T\mathbf{a}_T(\theta_D)|^2|\mathbf{a}_R^H(\theta)\mathbf{a}_R(\theta_D)|^2 \\ &= |\mathbf{a}_T^H(\theta)\mathbf{a}_T(\theta_D)+\mathbf{a}_T^H(\theta)\mathbf{\Gamma}^T\mathbf{a}_T(\theta_D)|^2|\mathbf{a}_R^H(\theta)\mathbf{a}_R(\theta_D)|^2 \\ &\geq |\mathbf{a}_T^H(\theta)\mathbf{a}_T(\theta_D)|^2|\mathbf{a}_R^H(\theta)\mathbf{a}_R(\theta_D)|^2 \\ &= G_{\mathrm{Tx,Rx_{Orth}}} \end{aligned} \quad (23)$$

where equation (23) follows from triangle inequality for complex numbers. ■

VI. Quantitative Analysis

In this section, we simulate the radar system and study the impact of null space projection on the radar waveform using the simulation parameters and setup of [1]. The null space of $\mathbf{H}$ is computed using SVD. Since $\mathbf{\Sigma}$ doesn't always have zero singular values, we take singular values below a certain threshold and take corresponding columns of $\mathbf{V}^H$. For example, SVD of $\mathbf{H}$ results in $\mathbf{\Sigma}$ with no zero singular values but the last two singular values are below a certain threshold so we take the columns of $\mathbf{V}^H$ corresponding to those singular values and then using (9) construct $\mathbf{P}_{\tilde{\mathbf{V}}}$. We transmit finite alphabet constant-envelope BPSK waveforms.

A. CRB

In this section, we compare the performance in terms of CRB for the two cases with or without confining the radar signal to the null space of $\mathbf{H}$ for 1000 realizations of a Rayleigh fading channel $\mathbf{H}$ of size $N_R \times M_T$. Using the simulation parameters mentioned in [1], the CRB on target direction estimation root-mean-square-error (RMSE) vs. SNR for a fixed θ and a single target is shown in Fig. 3 for different values of γ.

In Figure 3, the CRB for null space projected signal is high in RMSE as compared to the no null space projected signal. When $\gamma = 0$, the orthonormal waveform case, the RMSE is lowest possible for both original and projected waveforms, whereas, the $\gamma = 1$, the fully coherent waveform case, the RMSE is much higher than the orthonormal waveform case. The penalty in RMSE, is the direct result of constraint we are putting on radar signal that it should be in the null space of $\mathbf{H}$. Figure 3 shows that through projection we lose some

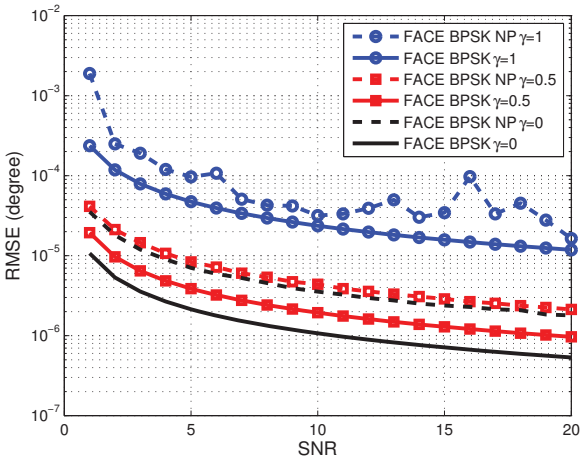

Fig. 3. CRB on target direction estimation RMSE as a function of the SNR.

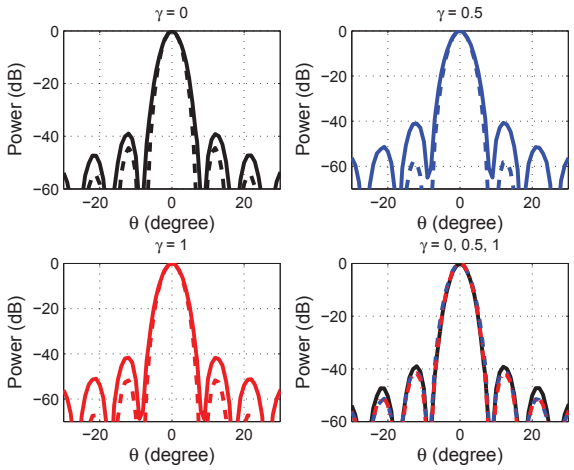

Fig. 4. Normalized transmit–receive beampatterns; $M_T = 9$ and $M_T = 9$; $M_R = 9$ transceiver elements with interelement spacing of $3\lambda/4$. The beams are digitally steered to $\theta_D = 0^\circ$ and the target is located at $\theta = 0^\circ$.

information. This might be critical information depending on the radar mission. Also, choice of radar waveform, value of parameter γ for FACE radar waveforms, plays an important role in the projection algorithm.

B. Beampattern

In this section, we analyze the beampatterns for different values of γ using the antenna setup of [1] for 5000 realizations of $\mathbf{H}$. We study the composite transmit-receive beampatterns because of their narrower null-to-null beamwidths and smaller sidelobes. Another advantage of studying composite beampatterns is that it gives an unambiguous beampattern due to presence of both transmit and receive beampatterns. If one pattern has an ambiguity, for example grating lobes, the other may resolve it [6].

When the radar signal is projected onto the null-space of $\mathbf{H}$, we get a modified radar signal with a new signal correlation matrix, see equation (18). The transmit-receive beampattern

for this new signal, solid lines, is shown in Fig. 4 along with the beampattern for original signal, dotted lines, for comparison for three values of γ. We observe that the shape of beampattern of null-projected signal doesn't change much except that we have sidelobes which are approximately 10 to 12 dB higher in magnitude. The null-to-null beamwidth of mainlobe and sidelobes, of null-projected waveform, are almost same as that of original radar waveform. Another important thing to note is that the projected waveform didn't steer the beam off the target and there is no beam shape loss thus guaranteeing the radar mission objectives.

C. MIMO Radar Antennas

In the previous work, we evaluated performance as we increased the number of radar antennas. We showed that the CRB improves more rapidly as the number of receive antennas is increased as compared to the transmit antennas. So in terms of radar performance we need to select optimal number of receive antennas to achieve desirable performance [1]. In this paper, we analyze the impact of radar antennas on beampattern. In Figure 5(a), we look at the shape of transmit-receive beampattern as we increase the MIMO radar transmit antennas. Increasing the number of transmit antennas has no effect on the null-to-null beamwidth of mainlobe and sidelobes. However, the magnitude of sidelobes do decrease. In Figure 5(b), we look at the shape of transmit-receive beampattern as we increase the MIMO radar receive antennas while keeping the transmit antennas of radar and communication system fixed. The important thing to note is that narrower null-to-null beamwidths of mainlobe and sidelobes can be achieved by increasing M_R even for null-projected waveforms without affecting the magnitude of sidelobes.

D. Threshold

In our previous work, we showed that by increasing the value of threshold the radar performance increases [1]. Recall that threshold is the limitation parameter in the projection algorithm and in the SVD of $\mathbf{H}$ those singular values are selected which are below the threshold. This means if the channel matrix has a large null space the radar performance won't be affected much.

In Figure 6, we analyze the effect of threshold value on the transmit-receive beampattern of null-projected radar waveform for $\gamma = 0$. As the threshold value increases the null-to-null beamwidth of the mainlobe and sidelobes stay the same. However, the magnitude of the sidelobes decreases. There is approximately a 5 dB drop in magnitude of sidelobes for every unit increase in the threshold value. Thus, selecting an optimal value for the threshold can limit the magnitude of the sidelobes.

E. Error

We define the error in the beampattern of the original radar waveform and the projected radar waveform as

$$\epsilon(\theta) \triangleq \frac{G_{\mathrm{Tx,Rx}}(\theta,\theta_D) - G_{\mathrm{Tx_{Null},Rx_{Null}}}(\theta,\theta_D)}{G_{\mathrm{Tx_{Null},Rx_{Null}}}(\theta,\theta_D)}, \qquad (24)$$

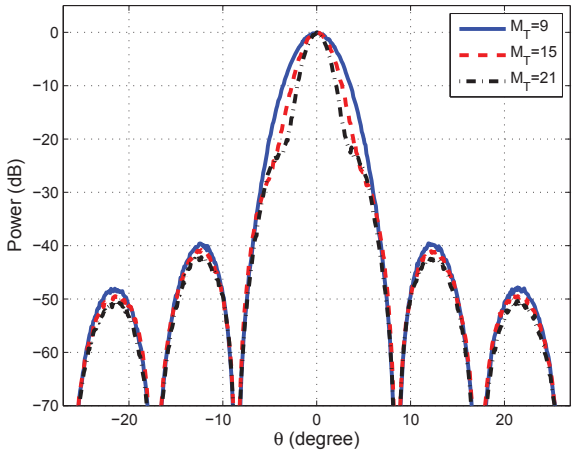

(a) $M_R = 9$ and $N_R = 9$.

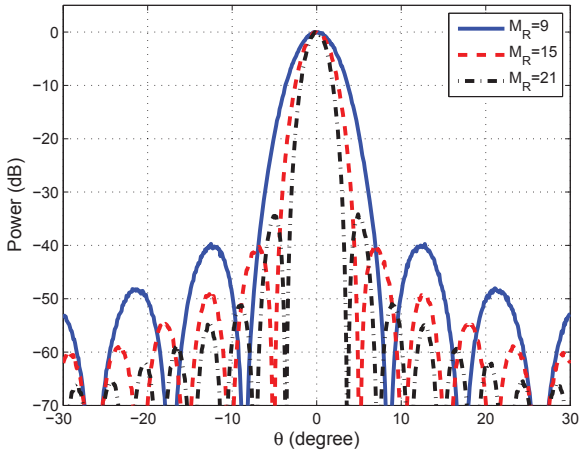

(b) $M_T = 9$ and $N_R = 9$.

Fig. 5. Normalized transmit–receive beampatterns using null-projected radar waveform; interelement spacing of $3\lambda/4$ between radar transceiver elements; and $N_R = 9$ communication system receive antennas. The beam is digitally steered to $\theta_D = 0^\circ$ and the target is located at $\theta = 0^\circ$.

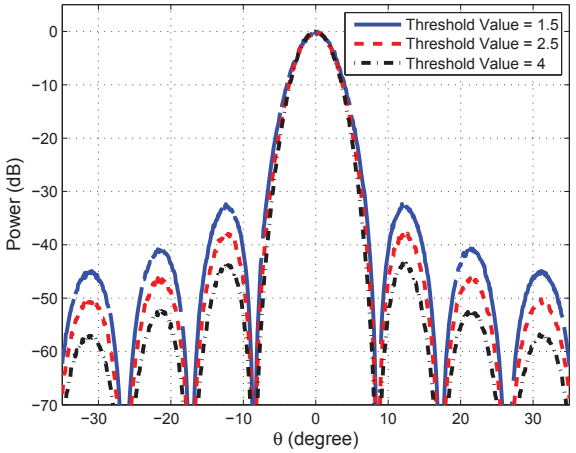

Fig. 6. Threshold impact on radar performance.

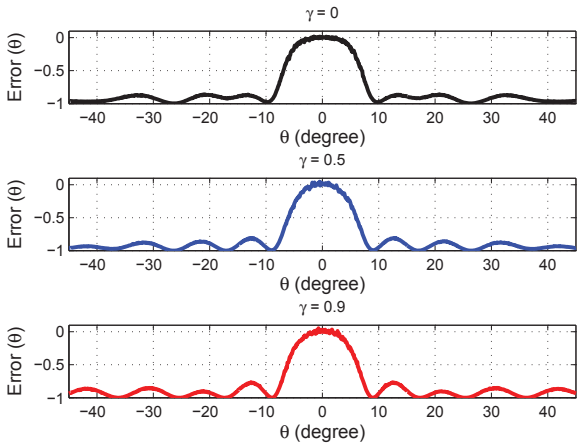

Fig. 7. Beampattern difference vs. θ for various γ.

TABLE I
TRANSMIT-RECEIVE BEAMPATTERN ANALYSIS

Radar Waveform	Parameter	Null-to-null Beamwidth	Magnitude of Sidelobes
Null-projected	$M_T \uparrow$ $M_R \uparrow$ Threshold $\uparrow$	Stays same $\downarrow$ Stays Same	$\downarrow$ Stays same $\downarrow$
FACE	$M_T M_R \uparrow$	$\downarrow$	$\downarrow$

where $\theta \in \{-45°, 45°\}$ and $\theta_D = 0°$. $\epsilon(\theta)$ describes the error in the transmit-receive beampattern for various angles when the beam is digitally steered to $\theta_D = 0°$ for the FACE waveform and its null projected version. This is shown in Figure 7 for various γ. Note that the difference between the original and projected waveform is zero for angles close to 0°, i.e the direction of digitally steered beam. Hence, the projection algorithm does not steer the beam off the target.

Hence, for the null-projected radar waveform we analyze the following trends, which are also summarized in Table I:

- Null-to-null beamwidth
  - stays same with the increase in number of radar transmit antennas M_T and/or threshold value, and
  - decreases with the increase in number of radar receive antennas M_R.
- Magnitude of sidelobes
  - decreases as we increase M_T,
  - stays same with the increase in number of radar receive antennas M_R, and
  - decreases with increase in the threshold value.

VII. CONCLUSION

In this paper, we designed a finite alphabet constant-envelope (FACE) radar waveform and projected it onto the null space of interference channel. We computed the CRB performance bound, for target direction estimation given that radar transmits FACE waveforms, for the two cases of projection onto null space and no null space projection. We showed that the loss in the performance of a radar in terms of RMSE is due to the projection of radar signals onto the null space of $\mathbf{H}$. We compared and analyzed the transmit-receive beampattern of original radar waveform and the null-projected radar waveform. We showed that both have the same null-to-null beamwidth but the null-projected waveform has higher sidelobes. We also showed that the null-projected waveform didn't steer the beam off the target and/or lose beam shape thus preserving radar mission objectives. Through simulation we showed that in order to preserve the radar performance in terms of RMSE we can optimally choose the number of receive antennas to compensate for the loss that projecting the radar signals onto the null space of the channel matrix can cause. In addition, we showed the impact of threshold selection, in the projection algorithm, on the performance of radar system. RMSE, of angle estimates, and magnitude of sidelobes, in the transmit-receive beampattern, can be decreased and brought to a reasonable level by the appropriate selection of threshold value.

The results derived in this paper show that null-space coexistence methods can work in the case of radar thus guaranteeing radar mission objectives. However, it comes with a cost when using null space based approach. The cost paid is more RMSE of radar target direction estimate and higher magnitude of sidelobes in the transmit-receive beampattern.

REFERENCES

[1] S. Sodagari, A. Khawar, T. C. Clancy, and R. McGwier, "A projection based approach for radar and telecommunication systems coexistence," in *Proc. IEEE Globecom*, 2012.

[2] A. Lackpour, M. Luddy, and J. Winters, "Overview of interference mitigation techniques between WiMAX networks and ground based radar," in *Proc. 20th Annual Wireless and Optical Comms. Conf.*, 2011.

[3] H. Deng and B. Himed, "Interference mitigation processing for spectrum-sharing between radar and wireless communications systems," *IEEE Transactions on Aerospace and Electronic Systems*, vol. 49, no. 3, pp. 1911–1919, 2013.

[4] F. H. Sanders, R. L. Sole, J. E. Carroll, G. S. Secrest, and T. L. Allmon, "Analysis and resolution of RF interference to radars operating in the band 27002900 MHz from broadband communication transmitters," Tech. Rep. 13-490, NTIA, October 2012.

[5] J. Li and P. Stoica, "MIMO radar with colocated antennas," *IEEE Signal Processing Magazine*, vol. 24, no. 5, pp. 106–114, 2007.

[6] J. Li and P. Stoica, *MIMO Radar Signal Processing*. Wiley-IEEE Press, 2008.

[7] S. Ahmed, J. S. Thompson, Y. R. Petillot, and B. Mulgrew, "Finite Alphabet Constant-Envelope Waveform Design for MIMO Radar," *IEEE Transactions on Signal Processing*, vol. 59, no. 11, pp. 5326–5337, 2011.

[8] H. Yi, H. Hu, Y. Rui, K. Guo, and J. Zhang, "Null space-based precoding scheme for secondary transmission in a cognitive radio MIMO system using second-order statistics," in *Proc. IEEE Intl. Comm. Conf.*, 2009.

[9] H. Yi, "Nullspace-based secondary joint transceiver scheme for cognitive radio MIMO networks using second-order statistics," in *Proc. IEEE Intl. Comms. Conf.*, 2010.

[10] M. Filo, A. Hossain, A. R. Biswas, and R. Piesiewicz, "Cognitive pilot channel: Enabler for radio systems coexistence," in *Proc. 2nd Intl. Workshop on Cognitive Radio and Advanced Spectrum Management*, 2009.

[11] T. S. Shores, *Applied Linear Algebra and Matrix Analysis*. Springer-Verlag New York, 2007.